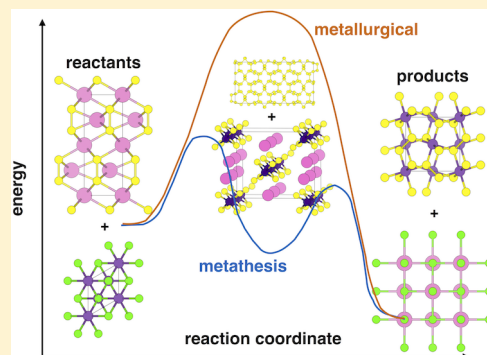


Pyrite Formation via Kinetic Intermediates through Low-Temperature Solid-State Metathesis

Andrew J. Martinolich and James R. Neilson*

Department of Chemistry, Colorado State University, Fort Collins, Colorado 80523-1872, United States

ABSTRACT: The preparation of materials with limited phase stabilities yet high kinetic activation barriers is challenging. Knowledge of their possible formation pathways aids in addressing these challenges. Metathesis reactions present an approach to circumvent these barriers; however, solid-state metathesis reactions are often too rapid from extensive self-heating to understand the reaction. The stoichiometric reaction of MCl_2 salts ($M = Mn, Fe, Co, Ni, Cu, Zn$) with Na_2S_2 enables the formation of pyrite (FeS_2), CoS_2 , and NiS_2 at low temperatures (250–350 °C). Na_2S_2 has the same polyanionic dimer as found in the pyrite structure, which would suggest the possibility of a facile ion-exchange reaction. However, from high-resolution synchrotron X-ray diffraction and differential scanning calorimetry, the energetic driving force does not appear to result solely from $NaCl$ formation but also from formation of intermediate and pyrite phases. It is apparent that the reaction proceeds through polyanionic disproportionation and formation of a low-density alkali-rich intermediate, followed by anionic comproportionation and atomic rearrangement into the pyrite phase. These results have profound implications for the use of low-temperature metathesis in achieving materials by design.



INTRODUCTION

The formation of solids illustrates the competition of thermodynamics and kinetics: while there is often a thermodynamic driving force to form a compound, the kinetic barriers from solid-state diffusion make design of materials extremely challenging.¹ Therefore, the solid-state chemist often relies on high-temperature reactions in order to produce a desired phase, assuming that the desired phase is thermodynamically stable. Alternatively, self-heating solid-state metathesis reactions have been used extensively in the formation of refractory and superhard compounds, such as sulfides, nitrides, borides, carbides, and silicides.^{2–6} With some precursors, the solid-state metathesis reaction does not proceed immediately with rapid self-heating and instead only proceeds with the application of heat over a period of time.⁷ Along these lines, metathesis has been integrated into aerosol-assisted formation pathways of nanomaterials.⁸ These formation pathways have also been used to form transition metal chalcogenide materials, and further integration of metathesis may allow control over the size and shape of resulting nanoparticles, which may in turn alter their properties as the crystallite size decreases.⁹ The use of solid-state metathesis at low temperatures, under conditions without extensive self-heating, presents many opportunities for the solid-state chemist to maintain increased control over reactions to master the formation of designer materials.

A compound of great interest for energy applications and geosciences is iron pyrite, FeS_2 . As a compound that melts incongruently ($T_{dec} = 743$ °C) and is comprised of high-melting iron and volatile sulfur, its preparation from the elements at ambient pressure can require long reaction times at high temperature and is not guaranteed to achieve stoichiometric

completion due to the formation of many other sulfur deficient compounds;^{10,11} excess sulfur is often used to generate the high fugacity needed to drive stoichiometric completion of the reaction.¹² Many transition metal disulfides form pyrite polymorphs, ranging across the period from MnS_2 to ZnS_2 ; however, MnS_2 , CuS_2 , and ZnS_2 are all high-pressure phases.^{13–15} The properties of pyrite change dramatically with metal substitution, ranging from antiferromagnetic insulators to superconductors.^{14,16–19} With the appropriate synthetic tools in hand, it may become possible to prepare novel related phases that would be otherwise unattainable through metallurgical preparatory routes.

Here, the salt-exchange metathesis reactions of metal dihalides with disodium disulfide



where M is a divalent 3d transition metal (Mn^{2+} , Fe^{2+} , Co^{2+} , Ni^{2+} , Cu^{2+} , and Zn^{2+}) are investigated. The formal reaction, as written, would correspond to a simple salt exchange, where the dimeric persulfide $[S_2]^{2-}$ polyanion exchanges two Na^+ cations for M^{2+} , as the pyrite lattice is comprised of the octahedral coordination of M^{2+} by $[S_2]^{2-}$ dimers (Figure 1).²⁰ This metathetical reaction at low temperature ($T_{rxn} = 350$ °C) yields formation of high-purity compounds that are thermodynamically stable at ambient pressures (FeS_2 , CoS_2 , and NiS_2). While this metathesis reaction reaches stoichiometric completion in the end, high-resolution synchrotron powder X-ray diffraction (HRSXRD) data suggest a far more complex mechanism than

Received: August 14, 2014

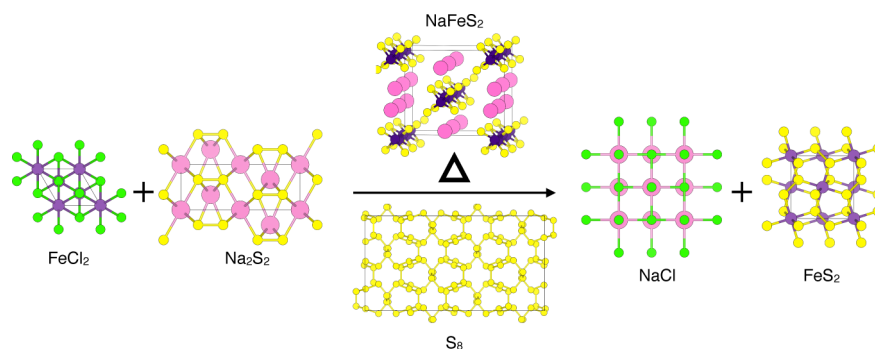


Figure 1. Schematic description of the metathesis reaction. Upon heating, iron chloride and disodium disulfide react to form sodium chloride and iron disulfide in the solid state. The reaction proceeds through metathesis, forming sodium iron sulfide and sulfur as reaction intermediates.

crystal chemistry would suggest, perhaps through reductive recombination to the elements or ionic exchange as previously hypothesized.^{2,7,21,22}

RESULTS

From differential scanning calorimetry (DSC), significant exothermic events occur on heating the reaction, even after the formation of NaCl (Figure 2a). Both thermodynamic and

formation is kinetically slow below 100 °C, due to the requisite diffusion through the solid matrix. Furthermore, a pressed pellet of FeCl₂ and Na₂S₂ slowly darkens from pale yellow to black over the course of ~2 months in either an inert or dry O₂ environment at room temperature, indicative that a reaction is taking place very slowly.

When an exotherm is triggered by heating to 175 °C, the reaction is far from complete, even after 24 h of equilibration, as indicated by the small mole fraction of FeS₂ visible in the product (Figure 2b,c and Table 1). At temperatures greater than 175 °C, there is sufficient thermal energy (for diffusion and other activated processes) as to allow for reaction completion.

HRSXRD of the reaction of FeCl₂ and Na₂S₂ at 350 °C reveals quantitative reaction completion and high-purity FeS₂. Rietveld analysis of the HRSXD data reveals 68.4(2) mol % NaCl and 30.4(2) mol % FeS₂ (Figure 3a). The remaining 1.3(2) mol % is monoclinic NaFeS₂.²³ The NaFeS₂ and NaCl were washed away with anhydrous methanol, which resulted in 99.63(1)% phase-pure pyrite FeS₂, along with a 0.37(7) mol % of Fe₇S₈ impurity (Figure 2b); this small phase fraction was further confirmed by determination of the ferromagnetic response of the sample, which also confirms less than 1 mol % of a Fe₇S₈ impurity.

The Fe₇S₈ phase was not observed in the diffraction data before washing and may have formed through decomposition of the NaFeS₂ or minor oxidation of the pyrite FeS₂ upon washing. Electronic transport measurements were performed on cold-pressed pellets and show an increase in resistivity upon cooling, confirming the material's bulk semiconducting nature.

While the reaction achieves stoichiometric completion by $T_{\text{rxn}} = 350$ °C (i.e., with seemingly little activation barrier), it does not do so through topochemical transformations or diffusive salt exchange. There is extensive redox chemistry that takes place, as indicated by the formation of several crystalline intermediates. HRSXRD data of the products from incomplete reactions ($T_{\text{rxn}} = 50$ and 175 °C) yield insight into the reaction pathway (Figure 2c). The diffraction patterns have appreciable, diffuse, noncrystalline backgrounds, as well as broad humps that sharpen at $T_{\text{rxn}} = 350$ °C and index to the expected reflections of monoclinic NaFeS₂. The observation of NaFeS₂ is surprising, as it would indicate the formal oxidation of Fe²⁺ to Fe³⁺ and reduction of [S₂]²⁻ to 2 S²⁻; there are no persulfide dimers in the structure of NaFeS₂ that would indicate a lesser negative charge on the sulfur.

At both intermediate temperatures, there are also numerous, sharp, low-Q reflections, all of which index to orthorhombic S₈,²⁵ suggesting that there is also formal oxidation of the [S₂]²⁻

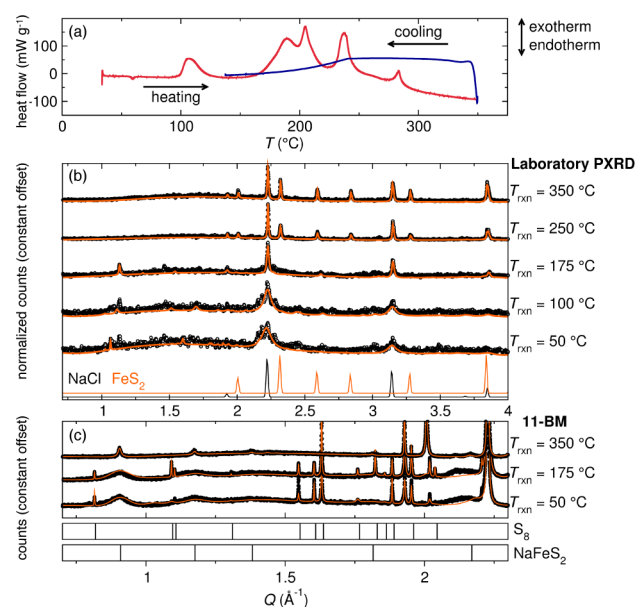


Figure 2. (a) DSC of the reaction of FeCl₂ with Na₂S₂ shows multiple exothermic processes as the temperature of the reaction increases. The data are normalized per gram of total reaction mixture. (b) PXRD patterns (black symbols) and corresponding fits determined through the Rietveld method (orange lines) of the reaction at the temperatures shown. NaCl formation is seen throughout, while FeS₂ is not seen until $T_{\text{rxn}} = 250$ °C. (c) HRSXRD patterns of the same reaction products show S₈ formation at low reaction temperatures, as well as a significant diffuse background component indicative of a disordered phase, which crystallizes into NaFeS₂. [Data plotted as $Q = 4\pi \sin(\theta)/\lambda$; $\lambda = 1.5418$ Å (b) and $\lambda = 0.41367$ Å (c).]

kinetic effects are required to reconcile the DSC and powder X-ray diffraction (PXRD) data. From PXRD of a 24 h reaction, NaCl forms by 50 °C (Figure 2b); however, the DSC trace with a heating rate of 1 °C min⁻¹ shows that all exothermic processes occur above ~100 °C (Figure 2a). This suggests that there is a low activation barrier for NaCl formation, but the

Table 1. Phase Fractions at Different Reaction Temperatures from Analysis of the Reaction Products of Eq 1 by High-Resolution Synchrotron PXRD (SXR) and Laboratory PXRD (PXR) for $M = \text{Fe}^{2+}$ and Co^{2+}

T_{rxn} , °C	$M = \text{Fe}^{2+}$; mol % (PXR/SXR)			
	NaCl	FeS_2	S_8	NaFeS_2
50	98(1)/86.1(1)	0/0	1.4(2)/7.25(3)	0.8(2)/6.70(5)
100	97(1)	0	3.0(3)	0.45(4)
175	88(2)/87.0(1)	0/3.49(5)	1.4(5)/3.97(3)	10.8(5)/5.59(4)
250	60(3)	39(2)	0	0
350	70(2)/68.3(1)	30(1)/30.37(6)	0/0	0/1.28(2)

T_{rxn} , °C	$M = \text{Co}^{2+}$; mol % (PXR)			
	NaCl	CoS_2	Na_2CoS_2	CoS
100	97(1)	0	2.5(7)	0
175	92(1)	0	8(1)	0.7(4)
250	85(2)	14(3)	0	0 ^a
350	73(1)	13(4)	0	11.0(9) ^b

^aAlso includes 0.36(4) mol % Co_9S_8 . ^bAlso includes 2.7(4) mol % Co_3S_4 .

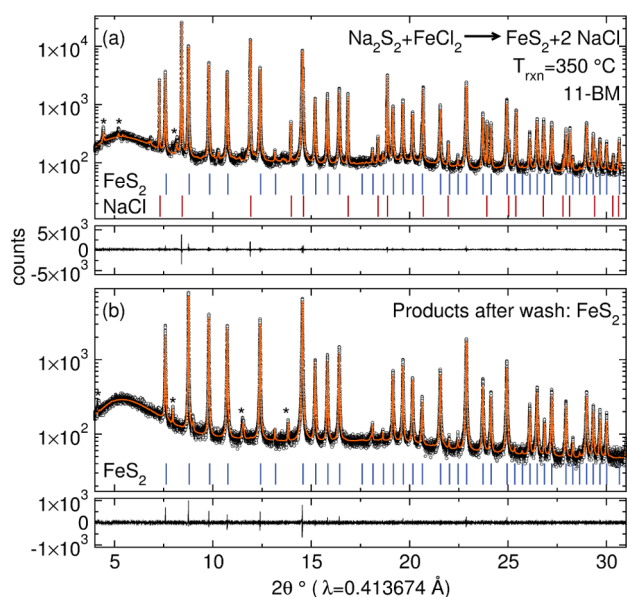


Figure 3. HRSXRD and Rietveld analysis of the products of reaction 1 (a) before and (b) after washing with anhydrous methanol, showing the data (black circles), calculated fit (orange lines), and difference between the two (black lines). Ticks below the data indicate expected reflections. Asterisks in part a denote monoclinic NaFeS_2 [1.3(2) mol %]. Asterisks in part b denote Fe_7S_8 [0.37(7) mol %]. Minority phases were incorporated into the refinements; their reflections were omitted for clarity.

to 2S^0 . However, crystalline sulfur is not present in the HRSXRD data of the 350 °C reaction and did not condense in the sealed ampule; this suggests that sulfur also participates as an intermediate in the reaction mechanism. By HRSXRD, no pyrite is observed at 50 °C, but crystallites are detected in the $T_{\text{rxn}} = 175$ °C products (Figure 2c, Table 1).

Similar trends are seen in the temperature-dependent reaction of CoCl_2 and Na_2S_2 (Figure 4). At low temperatures, Na_2CoS_2 is observed, which has an analogous structure to NaFeS_2 ; the extra sodium compensates for the divalent charge of Co^{2+} with sulfide (S^{2-}) anions. While comparable to the reaction with iron chloride, CoS_2 formation is more sensitive to temperature. At $T_{\text{rxn}} = 350$ °C, CoS_2 formation is accompanied by the sulfur-deficient phases CoS and Co_3S_4 . Despite CoS_2 being stable up to 950 °C,²⁶ progression through this reaction

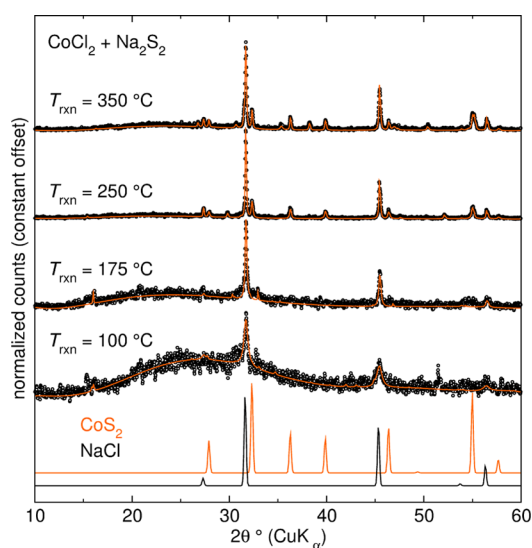
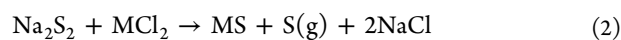


Figure 4. PXRD patterns of the products from the solid-state metathesis reactions of CoS_2 with Na_2S_2 (black circles) and corresponding Rietveld analyses (orange lines) at various temperatures. At low temperatures, S_8 and Na_2CoS_2 are detected. At increased temperatures, the formation of sulfur-deficient phases Co_3S_4 , CoS , and Co_9S_8 are detected, despite the stability of CoS_2 up to 950 °C.

pathway may be altered by the increased mobility of the sulfur. As the reaction temperature is increased, we infer that the volatilization of the sulfur intermediate overcomes the favorability of CoS_2 formation, leading to these sulfur-deficient phases.

In reactions with MCl_2 , ($M = \text{Mn}, \text{Fe}, \text{Co}, \text{Ni}, \text{Cu},$ and Zn), only FeS_2 , CoS_2 , and NiS_2 pyrite are formed (Figure 5). Only these pyrite-type compounds are found on the binary phase diagrams determined for near ambient pressures.^{10,26–30} While pyrite MS_2 phases have been reported at nonambient pressures for manganese, copper, and zinc,^{13–15} the thermodynamically favorable phases of MnS , CuS , and ZnS are observed, with the remnant sulfur condensing on the side of the ampule as it cooled according to the reaction



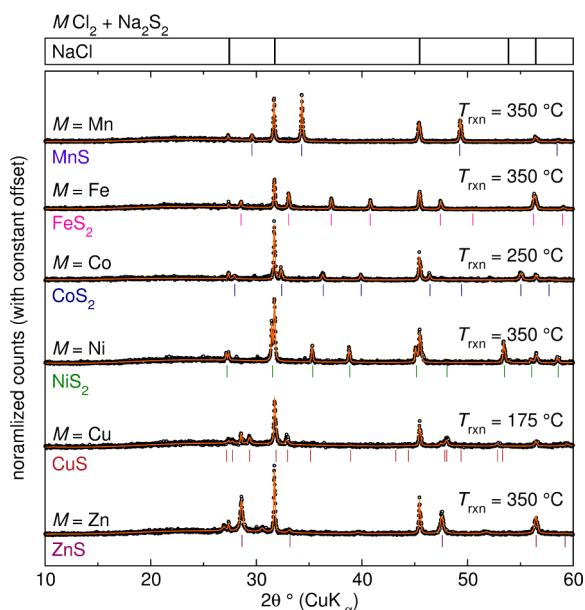


Figure 5. PXRD patterns of the products from the solid-state metathesis reactions of divalent transition metal chlorides with Na_2S_2 (black circles) and corresponding Rietveld analyses (orange lines) display the formation of either MS or MS_2 , as shown by the expected reflections under each pattern. The formation of NaCl is conserved. CuCl and wurtzite ZnS were also incorporated into the respective Rietveld refinements; ticks were omitted for clarity.

The reaction with ZnCl_2 produced a mixture of the high- and low-temperature polymorphs of ZnS , with the wurtzite and zinc blende structures, as previously shown.⁷

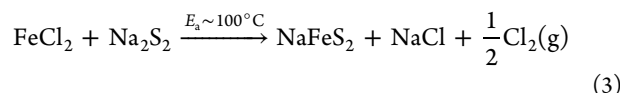
DISCUSSION

By correlating features in the DSC to changes in the observed phases, we can elucidate the elusive mechanism for these low-temperature solid-state metathesis reactions. Primarily, the melting or decomposition of any reagents during the reaction can be ruled out. Na_2S_2 does not decompose until 470 °C, and FeCl_2 does not melt or decompose until 677 °C.^{31,32} While Na_2S_2 undergoes a structural phase transition at 170 °C,³¹ crystalline Na_2S_2 is not observed in any of the X-ray diffraction patterns. This precludes formation of either S^{2-} or Fe^{3+} ions through decomposition of the reactants and must result from their reaction.

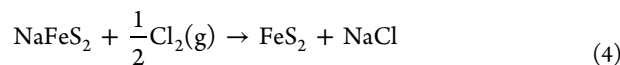
Sodium chloride provides a driving force to initiate the reaction; however, it does not provide a force to drive the reaction to completion. NaCl formation is observed by XRD at lower temperatures ($T_{\text{rxn}} = 50$ °C) than the exothermic release just above $T = 100$ °C observed from DSC (Figure 2). Furthermore, the exothermic processes shown here contrast the formation of pyrite NiS_2 from the previously reported metathesis reaction of K_2NiF_6 and $2\text{Na}_2\text{S}_5 \cdot 0.06\text{H}_2\text{O}$. There, a vigorous exothermic reaction occurs around $T_{\text{rxn}} \sim 65$ °C, with a peak heat flow of ~ 1700 mW g^{-1} .²¹ Here, the maximum heat flow is ~ 200 mW g^{-1} , reflecting a weaker overall driving force and the ability to follow the reaction intermediates. Taken together, these results indicate that a small amount of thermal energy is required for diffusion, which is sufficient to initiate the formation of NaCl , but not the pyrite phase.

The exothermic release just above $T = 100$ °C corresponds to the formation of NaCl and of a poorly ordered NaFeS_2 phase. In the DSC experiment, the heating rate was 1 °C/min,

which is not likely slow enough to observe completion formation of NaCl below 100 °C; therefore, the formation of NaCl at lower temperatures is not likely. Furthermore, there is a significant increase in the NaCl diffraction intensity (with a decrease in peak width) when comparing the $T_{\text{rxn}} = 50$ and 175 °C diffraction data. The same trend is observed during the formation of CoS_2 (Figure 4). The comparison of the products from these two reaction temperatures also shows a significant increase in the amount of NaFeS_2 (or Na_2CoS_2) present in the product (Table 1). Furthermore, there is not a substantial increase in the intensity of the diffraction from NaCl between the $T_{\text{rxn}} = 175$ and 350 °C diffraction data in either the iron- or cobalt-containing products; however, quantification of this change is not straightforward. Together, these imply that the initial exotherm is the initiation of the reaction through formation of NaCl and NaFeS_2 (or Na_2CoS_2), with a low activation barrier that is rapidly overcome by heating to 100 °C:



The theoretical enthalpy of this reaction is $\Delta H_{\text{rxn}} = -2.8$ kJ mol^{-1} (since $\Delta H_f^\circ(\text{NaFeS}_2) = -331.3$ kJ mol^{-1}).³³ Such a reaction is barely exothermic, which would explain the small exotherm observed in DSC that is concomitant with the observation of NaFeS_2 and NaCl . The thermochemistry of the reaction



is strongly exothermic relative to eq 3, as $\Delta H_{\text{rxn}} = -258.4$ kJ mol^{-1} . The presence (or absence of) $\text{Cl}_2(\text{g})$ [or $\text{S}_8(\text{s})$] does not influence the thermochemical calculation; therefore, it is clear that the significant exotherm observed above $T > 175$ °C must arise from the formation of FeS_2 and NaCl .

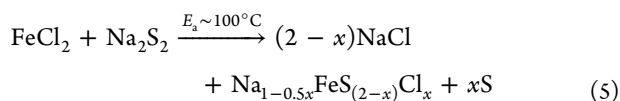
From a control reaction, it was confirmed that Cl_2 gas is not evolved. The reaction was performed in the presence of a sodium metal getter, with the reaction mixture in a crucible on top of a crucible containing the sodium and both crucibles sealed into an evacuated SiO_2 ampule. The expectation would be that if chlorine gas were being produced, NaCl would form on the surface of the liquid sodium metal. After reaction at 350 °C for 24 h, no NaCl was formed, but instead Na_2S was found in the getter crucible. Accordingly, the reaction mixture of FeCl_2 and Na_2S_2 formed FeS and NaCl . Since Cl_2 was not detected, it provides evidence that the chlorine must be integrated into the low-density NaFeS_2 intermediate.

After heating the mixture of Na_2S_2 and FeCl_2 at 175 °C for 24 h, one observes NaFeS_2 , S_8 , and NaCl . From the analysis of density functional theory calculations, NaFeS_2 is reported to be unstable with respect to decomposition into FeS_2 , FeS , and Na_2S .³⁴ This is further confirmed by our attempts to prepare NaFeS_2 , which were unsuccessful. Preparation of related compounds is best achieved by reaction of the alkali with the transitional metal chalcogenide as a pre-reaction, followed by homogenization and reaction at elevated temperature.^{35–39} Reaction of FeS_2 with sodium metal yielded only FeS_2 , Na_2S , and a sulfur-deficient $\text{FeS}_{(2-x)}$ phase. Instead, preparation of NaFeS_2 requires the leaching of aqueous suspensions or electrochemical means.^{23,24,33} These findings further implicate NaFeS_2 as an intermediate phase in the reaction.

Collectively, these data provide insight into the complete mechanism of pyrite formation via metathesis. The metathesis

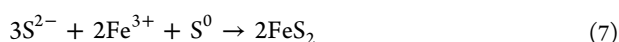
reaction does not appear to be limited by solid-state diffusion, even at room temperature, and the reaction does not appear to be susceptible to thermal runaway. Rather than the simple salt exchange between Fe^{2+} and $[\text{S}_2]^{2-}$, there appears to be a more complicated reaction mechanism predicated on the formation of low-density crystalline intermediates. From XRD, it is apparent that NaCl forms first, while the Fe and S combine to form the intermediates NaFeS_2 and S: $\text{FeCl}_2 + \text{Na}_2\text{S}_2 \rightarrow x\text{NaCl} + y\text{NaFeS}_2 + z\text{S} \rightarrow \text{FeS}_2 + 2\text{NaCl}$. However, this does not stoichiometrically balance with chlorine, and chlorine gas was not detected.

Therefore, we speculate that the reaction may proceed through the formation of NaCl and attack of the FeCl_2 lattice by sulfur through disproportionation of the persulfide anion, $[\text{S}_2]^{2-} \rightarrow \text{S}^{2-} + \text{S}^0$:



The first step, eq 5, has a low activation barrier; it can take place even at room temperature over the course of several months. Evidence in favor of such a mechanism with the incorporation of Cl into NaFeS_2 is provided by the poor crystallinity of the observed NaFeS_2 phase, in addition to the distinct, larger lattice parameters of the monoclinic NaFeS_2 phase relative to the previously reported compound, as to accommodate the Cl^- ions, which provide less electrostatic screening between metal cations.^{40,41} Such a mechanism, derived by considering only the observed crystalline products, requires just partial oxidation of Fe^{2+} to Fe^{3+} during the early stages of FeCl_2 attack, as the iron valence is given by $\text{Fe}^{(3-x/2)+}$, where x is given in eq 5. However, our observations and analysis do not preclude the formation of additional amorphous intermediates.

Furthermore, these redox activities can be rationalized as a reaction between the two intermediates, elemental sulfur and NaFeS_2 . Comproportionation of the sulfur can occur when the S^{2-} anion reduces both the Fe^{3+} and S^0 to form pyrite:



From Rietveld refinements of the HRSPXRD data, the nominal ratios of $\text{Fe}^{3+}:\text{S}^{2-}:\text{S}^0$ are 1:2:1 at 50 °C and 1.375:2.75:1 at 175 °C. Therefore, discrepancies between the stoichiometry of the balanced chemical reaction and the observed values may be attributed to the poor crystallinity or sulfur deficiency of the NaFeS_2 intermediate.

The removal of NaFeS_2 is predicated on the formation of NaCl, which leads to the formation of FeS_2 . The reactions with $\text{M} = \text{Co}^{2+}$ or Ni^{2+} also have suitable intermediates with the alkali-rich phases related to the structures of Na_2CoS_2 or $\text{K}_2\text{Ni}_3\text{S}_4$, the former of which was detected in the low-temperature reactions of CoCl_2 and Na_2S_2 . The resulting metal sulfides are all thermodynamically stable phases at ambient pressure, but not necessarily at ambient temperature, as shown by the formation of both zinc blende and wurtzite ZnS , along with NaCl and sulfur. This reveals the possibility of a synthetically controlled route toward formation of nonambient and ambient phases through metathesis.

CONCLUSION

Solid-state metathesis can be used to prepare pyrite metal disulfides at low temperature and without extensive self-heating or thermal runaway. While robust for a number of other transition metal disulfides, it appears that a major driving force for product formation is not primarily the formation of the metathesis byproduct, NaCl. Instead, from a combination of HRSXRD and DSC, formation of the thermodynamically stable pyrite phases drives the overall reaction, while a low activation barrier for NaCl formation and favorable intermediate formation enables initiation of the reaction, without extensive self-heating. Through careful analysis of the reaction intermediates, the metathesis involves significant atomic rearrangements in the formation of alkali-rich metal sulfides at low temperatures. This approach provides wide implications for the preparation of novel compounds or low decomposition temperature materials that have substantial activation barriers that prevent their facile formation.

EXPERIMENTAL SECTION

All reagents were purchased from Sigma-Aldrich or NOAH Technologies at a purity of 98% or higher. Sulfur was additionally purified through vapor transport in an evacuated sealed tube with a temperature gradient from 550 to 400 °C. The impurities were left in the hot end of the tube while sulfur condensed in the cooler end of the tube as the vessel cooled.

Na_2S_2 was prepared from the elements in a manner with which to avoid direct contact of the elements, which could produce an exothermic thermite reaction. In an argon-filled glovebox, sodium and sulfur were placed in separate alumina crucibles and sealed in the same silica tube, with the sulfur on top. The tube was then evacuated to <10 mTorr and sealed without exposure to the atmosphere. The tube was then heated to 200 °C for 24 h to allow sulfur vapor to corrode the sodium. The resulting heterogeneous solid was homogenized and pelleted in the glovebox, resealed, and heated for an additional 12 h at 300 °C.

For the solid-state metatheses of MS_2 , anhydrous MCl_2 and Na_2S_2 were ground to a homogeneous powder and pelletized in an argon-filled glovebox. The pellet was then placed in an alumina crucible and sealed in a quartz tube, evacuated to <10 mTorr without exposure to the atmosphere. The reaction vessel was then heated at 1 °C min^{-1} in a box furnace to the specified temperature for 24 h and the furnace cooled. The product was then recovered in an argon glovebox, washed five times with anhydrous methanol under an inert atmosphere using Schlenk techniques, dried under vacuum at room temperature, and then recollected in the glovebox.

Purity of the Na_2S_2 was confirmed by X-ray diffraction using a Bruker APEX II single crystal diffractometer (Mo $K\alpha$ radiation, $\lambda = 0.7107$ Å) with powder in a sealed quartz capillary; the two-dimensional data were radially integrated for analysis. Powder X-ray diffraction data (PXRD) were collected on a Scintag X-2 diffractometer with Cu $K\alpha$ radiation. High-resolution synchrotron powder X-ray diffraction data were collected from powders sealed in quartz capillaries loaded into Kapton capillaries on the beamline 11-BM-B ($\lambda = 0.413673$ Å).⁴² Rietveld analyses were performed using EXPGUI/GSAS.^{43,44} Physical properties measurements were performed using a Quantum Design, Inc. Dynacool PPMS, using the electronic transport option and vibrating sample magnetometer. Differential scanning calorimetry was performed on samples hermetically sealed in the glovebox using a TA Instruments 2920 modulated DSC with a 1 °C min^{-1} ramp rate in order to replicate the reaction conditions.

AUTHOR INFORMATION

Corresponding Author

james.neilson@colostate.edu

Notes

The authors declare no competing financial interest.

ACKNOWLEDGMENTS

The authors thank the excellent staff at the 11-BM-B beamline for their rapid and efficient collection of the synchrotron X-ray diffraction data. The research reported in this publication was supported by the Energy Institute at Colorado State University. Use of the Advanced Photon Source at Argonne National Laboratory was supported by the U.S. Department of Energy, Office of Science, Office of Basic Energy Sciences, under Contract No. DE-AC02-06CH11357.

REFERENCES

- (1) Committee for an Assessment of and Outlook for New Materials Synthesis and Crystal Growth, National Research Council (US). *Frontiers in Crystalline Matter: From Discovery to Technology*; The National Academies Press: Washington, DC, 2009.
- (2) Bonneau, P. R.; Jarvis, R. F.; Kaner, R. B. *Nature* **1991**, *349*, 510–512.
- (3) Gillan, E. G.; Kaner, R. B. *Chem. Mater.* **1996**, *8*, 333–343.
- (4) Chung, H.-Y.; Weinberger, M. B.; Levine, J. B.; Kavner, A.; Yang, J.-M.; Tolbert, S. H.; Kaner, R. B. *Science* **2007**, *316*, 436–439.
- (5) Nartowski, A. M.; Parkin, I. P.; Craven, A. J.; MacKenzie, M. *Adv. Mater.* **1998**, *10*, 805–808.
- (6) Parkin, I. P. *Chem. Soc. Rev.* **1996**, *25*, 199–207.
- (7) Shaw, G. A.; Morrison, D. E.; Parkin, I. P. *J. Chem. Soc., Dalton Trans.* **2001**, 1872–1875.
- (8) Mann, A. K. P.; Skrabalak, S. E. *Chem. Mater.* **2011**, *23*, 1017–1022.
- (9) Motl, N. E.; Mann, A. K. P.; Skrabalak, S. E. *J. Mater. Chem. A* **2013**, *1*, 5193–5202.
- (10) Waldner, P.; Pelton, A. *J. Phase Equilib. Diffus.* **2005**, *26*, 23–38.
- (11) Yu, L.; Lany, S.; Kykyneshi, R.; Jieratum, V.; Ravichandran, R.; Pelatt, B.; Altschul, E.; Platt, H. A. S.; Wager, J. F.; Keszler, D. A.; Zunger, A. *Adv. Energy Mater.* **2011**, *1*, 748–753.
- (12) Seefeld, S.; Limpinsel, M.; Liu, Y.; Farhi, N.; Weber, A.; Zhang, Y.; Berry, N.; Kwon, Y. J.; Perkins, C. L.; Hemminger, J. C.; Wu, R.; Law, M. *J. Am. Chem. Soc.* **2013**, *135*, 4412–4424.
- (13) Bither, T.; Prewitt, C.; Gillson, J.; Bierstedt, P.; Flippen, R.; Young, H. *Solid State Commun.* **1966**, *4*, 533–535.
- (14) Bither, T. A.; Bouchard, R. J.; Cloud, W. H.; Donohue, P. C.; Siemons, W. J. *Inorg. Chem.* **1968**, *7*, 2208–2220.
- (15) Bither, T.; Donohue, P.; Cloud, W.; Bierstedt, P.; Young, H. *J. Solid State Chem.* **1970**, *1*, 526–533.
- (16) Corliss, L. M.; Elliott, N.; Hastings, J. M. *J. Appl. Phys.* **1958**, *29*, 391–392.
- (17) Ennaoui, A.; Tributsch, H. *Sol. Cells* **1984**, *13*, 197–200.
- (18) Cheng, S. F.; Woods, G. T.; Bussmann, K.; Mazin, I.; Soulen, R. J., Jr.; Carpenter, E.; Das, B.; Lubitz, P. *J. Appl. Phys.* **2003**, *93*, 6847–6849.
- (19) Gautier, F.; Krill, G.; Lapierre, M.; Panissod, P.; Robert, C.; Czjzek, G.; Fink, J.; Schmidt, H. *Phys. Lett. A* **1975**, *53*, 31–33.
- (20) Goodenough, J. B. *J. Solid State Chem.* **1971**, *3*, 26–38.
- (21) Bonneau, P. R.; Shibao, R. K.; Kaner, R. B. *Inorg. Chem.* **1990**, *29*, 2511–2514.
- (22) Bonneau, P. R.; Jarvis, R. F.; Kaner, R. B. *Inorg. Chem.* **1992**, *31*, 2127–2132.
- (23) Taylor, P.; Shoesmith, D. W. *Can. J. Chem.* **1978**, *56*, 2797–2802.
- (24) Taft, C. A. *J. Phys. (Paris)* **1977**, *38*, 1161–1162.
- (25) Abrahams, S. C. *Acta Crystallogr.* **1955**, *8*, 661–671.
- (26) Kuznetsov, V.; Sokolova, M.; Palkina, K.; Popova, Z. *Inorg. Mater.* **1965**, *1*, 617–632.
- (27) Franzen, H. In *Binary Alloy Phase Diagrams*, 2nd ed.; Massalski, T., Ed.; 1990; Vol. 3, pp 2593–2597.
- (28) Waldner, P.; Pelton, A. D. *Z. Metallkd.* **2004**, *95*, 672–681.
- (29) Lee, B.-J.; Sundman, B.; Kim, S. I.; Chin, K.-G. *ISIJ Int.* **2007**, *47*, 163–171.
- (30) Sharma, K.; Chang, Y. *J. Phase Equilib.* **1996**, *17*, 261–266.
- (31) Sangster, J.; Pelton, A. *J. Phase Equilib.* **1997**, *18*, 89–96.
- (32) Patnaik, P. *Handbook of Inorganic Chemicals*; McGraw-Hill: New York, 2003.
- (33) Lassin, A.; Piantone, P.; Crouzet, C.; Bodéan, F.; Blanc, P. *Appl. Geochem.* **2014**, *45*, 14–24.
- (34) Jain, A.; Ong, S. P.; Hautier, G.; Chen, W.; Richards, W. D.; Dacek, S.; Cholia, S.; Gunter, D.; Skinner, D.; Ceder, G.; Persson, K. A. *APL Mater.* **2013**, *1*, 011002.
- (35) Neilson, J. R.; McQueen, T. M. *J. Am. Chem. Soc.* **2012**, *134*, 7750–7757.
- (36) Caron, J. M.; Neilson, J. R.; Miller, D. C.; Llobet, A.; McQueen, T. M. *Phys. Rev. B* **2011**, *84*, 180409(R).
- (37) Caron, J. M.; Neilson, J. R.; Miller, D. C.; Arpino, K. E.; Llobet, A.; McQueen, T. M. *Phys. Rev. B* **2012**, *85*, 180405(R).
- (38) Neilson, J. R.; Llobet, A.; Stier, A. V.; Wu, L.; Wen, J.; Tao, J.; Zhu, Y.; Tesanovic, Z. B.; Armitage, N. P.; McQueen, T. M. *Phys. Rev. B* **2012**, *86*, 054512.
- (39) Neilson, J. R.; McQueen, T. M.; Llobet, A.; Wen, J.; Suchomel, M. R. *Phys. Rev. B* **2013**, *87*, 045124.
- (40) Boller, H.; Blaha, H. *Monatsh. Chem.* **1983**, *114*, 145–154.
- (41) Neilson, J.; Kurzman, J.; Seshadri, R.; Morse, D. *Chem.—Eur. J.* **2010**, *16*, 9998–10006.
- (42) Wang, J.; Toby, B. H.; Lee, P. L.; Ribaud, L.; Antao, S. M.; Kurtz, C.; Ramanathan, M.; Von Dreele, R. B.; Beno, M. A. *Rev. Sci. Instrum.* **2008**, *79*, 085105.
- (43) Toby, B. H. *J. Appl. Crystallogr.* **2001**, *34*, 210–213.
- (44) Larson, A.; Von Dreele, R. *General Structure Analysis System (GSAS)*; Los Alamos National Lab: Los Alamos, NM, 2004.